applied sciences

MDPI

Article

Power Losses Minimization for Optimal Operating Maps in Power-Split HEVs: A Case Study on the Chevrolet Volt

Antonella Castellano and Marco Cammalleri *

Department of Engineering, University of Palermo, 90128 Palermo, Italy; antonella.castellano@unipa.it
* Correspondence: marco.cammalleri@unipa.it

Abstract: The power-split architecture is the most promising hybrid electric powertrain. However, a real advantage in energy saving while maintaining high performance can be achieved only by the implementation of a proper energy management strategy. This requires an optimized functional design before and a comprehensive analysis of the powertrain losses after, which could be rather challenging owing to the constructive complexity of the power-split transmission, especially for multi-mode architecture with multiple planetary gearing. This difficulty was overcome by a dimensionless model, already available in the literature, that enables the analysis of any power-split transmission, even in full electric operation. This paper relies on this approach to find the operating points of the internal combustion engine and both electric machines which minimize the total power losses. This optimization is carried out for given vehicle speed and demanded torque, by supposing different scenarios in respect of the battery capability of providing or gathering power. The efficiency of the thermal engine and the electric machines is considered, as well as the transmission mechanical power losses. The aim is to provide a global efficiency map that can be exploited to extract data for the implementation of the most suitable real-time control strategy. As a case study, the procedure is applied to the multi-mode power-split system of the Chevrolet Volt.

Keywords: hybrid electric vehicles; power-split powertrain; global efficiency; multi-mode transmission; Voltec analysis

Citation: Castellano, A.; Cammalleri, M. Power Losses Minimization for Optimal Operating Maps in Power-Split HEVs: A Case Study on the Chevrolet Volt. *Appl. Sci.* **2021**, *11*, 7779. https://doi.org/10.3390/app11177779

Academic Editor: Maria Grazia De Giorgi

Received: 29 July 2021
Accepted: 19 August 2021
Published: 24 August 2021

1. Introduction

In the last decades, stricter environmental policies undertaken against increasing global warming have encouraged the spreading uptake of hybrid electric vehicles. Besides the earliest and most popular series and parallel hybrid architectures, more and more automotive companies—first and foremost Toyota and General Motors—are developing the power-split hybrid electric powertrain [1–5].

The power-split layout combines the benefits of both series and parallel hybrid, resulting in a highly flexible system where the internal combustion engine (ICE) is kinematically decoupled by the wheels due to the operation of the electric unit. Two electric machines act as an active continuously variable unit (CVU), which can provide additional power for vehicle propulsion or gather the ICE power in surplus for battery recharging. In addition, regenerative braking and full electric vehicle (FEV) operation are achievable. The power flows within the powertrain are handled by a power-split unit (PSU) made up of planetary gear sets (PGs) and ordinary gear sets (OGs). Multi-PG PSU enables the minimization of the electric machines' power size by deploying a multi-mode power-split continuously variable transmission (PS-CVT), where some clutches operations lead to several constructive arrangements to select under the desired driving conditions [6–10]. Nevertheless, the more complex the transmission constructive layout is, the trickiest the identification of the occurring power flows is [11–13], as well as their management [14–17].

When implementing energy management strategies aimed at minimizing the powertrain power losses, the friction losses occurring in the transmission should be also considered. Nonetheless, because of the above-mentioned difficulties in multi-mode PS-CVTs

analysis, their calculation is far from trivial [18–21]. Thus, mechanical power losses are considered in very simple one-PG transmission [22,23] or evaluated by using simplified approaches that avoid the analysis of the transmission power flows [24,25] or even more often neglected [26–32].

The focus of this paper is to provide the global efficiency map of the multi-mode Chevrolet Volt hybrid electric powertrain by assessing all powertrain losses, not only those occurring in the propulsors but also the transmission mechanical power losses. This can be achieved by applying a unified parametric model [33–36] without convoluted or case-specific formulations. All the relationships of the model are ruled by few basic functional parameters which can be swiftly derived from any PS-CVT constructive arrangement, even multi-PG or multi-mode [34,36]. These enable the calculation of speed, torque, and power ratios in real conditions, by using a fast black-box method [35,36] to assess the PSU mechanical losses and then the actual power that the electric machines should provide to the PSU for given ICE power and required output. The whole procedure applies also to the FEV operation [36].

This unified parametric model was first applied to the transmission of the Chevrolet Volt in [34], where an alternative design was proposed but any power losses were neglected. Then, the mechanical losses occurring in the PSU were considered in the Chevrolet Volt dimensionless analysis carried out in [35]. This article aims to consider also the power losses occurring in the propulsors, by moving from the dimensionless variables to those expressed in physical units of measurement. In addition, the analysis of the Chevrolet Volt in FEV operation is presented for the first time.

The utilization of dimensionless independent and dependent variables expressed as speeds, torques, or powers ratios results in utmost generality, which makes the model suitable for analyzing any PS-CVT. Nonetheless, the loss factors of the propulsors are strictly related to their operating point, therefore the brake specific fuel consumption (BSFC) map of the engine and the efficiency maps of the electric machines have to be introduced. By considering different combinations of input and output speeds and torques, it is possible to investigate the powertrain response in terms of the actual functioning point of the propulsors and related power losses, net power flow provided or gathered by the battery, and powertrain global efficiency. This approach outputs the results in some optimal operating maps collecting all data of interest, which allows the determination of the powertrain optimal functioning points based on the desired goal of the energy management strategy to implement. By way of example, this contribution proposes a simplified control strategy in steady-state driving by taking into consideration four possible state of charges (SOCs) of the battery. However, this approach is the ideal basis for the development of new control and energy management strategies, as it applies to any hybrid electric powertrain without requiring an in-deep knowledge of the behavior of each component of the powertrain, thanks to its generality. Therefore, it offers a neutral environment for engineers with different expertise.

The paper is organized as follows. Section 2 includes the dimensionless PSU mechanical power losses and the dimensionless speeds and real powers of the electric machines in the Chevrolet Volt powertrain in power-split operation, which were previously calculated in [35]. Then, the same variables are evaluated in FEV operation by using the procedure presented in [36]. In Section 3, the propulsors efficiency maps are introduced and the method for calculating and selecting the optimal operating points is described. Section 4 provides and discusses the results of the application, while Section 5 concludes the article by framing the new contribution in a broader context.

2. Dimensionless Parametric Approach for Voltec Analysis

The transmission system of the Chevrolet Volt, the so-called Voltec, is a PS-CVT with two PGs and three clutches which enable the multi-mode functioning. A third PG combined with a chain drive acts as a fixed-ratio OG in the final drive. Figure 1 shows the Voltec functional layout derived from [37] and previously described in [34,35]. The PGs and the

final drive make up the PSU, which can be considered as a four-port device linked with the ICE (by the shaft *in*), the wheels (by the shaft *out*), and the electric motor-generator (MG) I (by the shaft *i*) and MG O (by the shaft *o*). The positive sign of the power flows is indicated by the arrows. The clutches C0, C1, and C2 are exploited to shift between different modes, as reported in Table 1. By engaging the only C2 clutch, the PG2 ring gear is braked to the frame, thus only PG1 acts as an epicyclic gear unit with non-proportional speeds of its branches. This realizes an input-split mode, mainly exploited for lower vehicle speeds. At higher speeds, a compound-split mode is achieved, by engaging only the clutch C1 which connects the PG2 ring gear to the MG I and the PG1 sun gear. It should be noted that engaging C1 and C2 simultaneously realizes a fixed-ratio parallel mode, where only MG O can be active and the ICE speed is univocally coupled to the vehicle speed. Moreover, by additionally engaging the one-way clutch C0, which locks to the frame the ICE and the PG1 ring gear, two FEV modes can be performed. However, as shown in Table 1, General Motors considers only the FEV operation derived from the input-split arrangement.

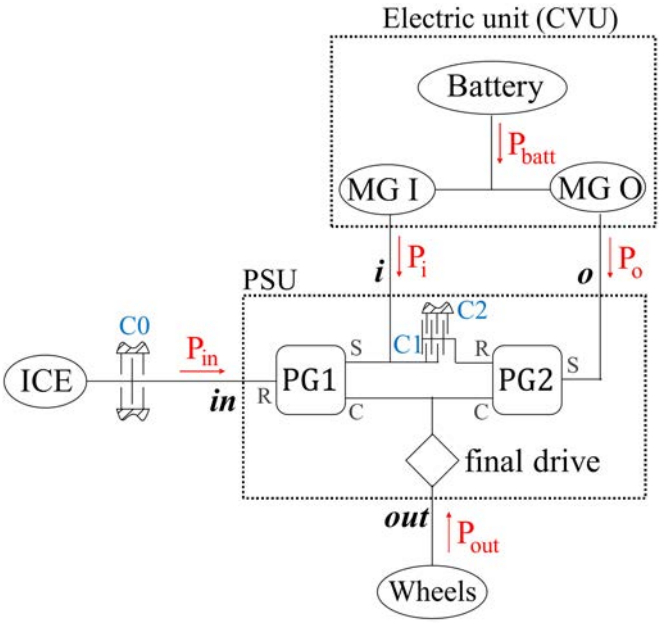

Figure 1. Functional layout of Voltec. The PGs ring gear, sun gear, and carrier are indicated by R, S, and C, respectively. Red arrows indicate the positive direction of power flows. Clutches are indicated by blue labels.

Table 1. Clutches operations for Voltec operating modes provided by General Motors.

Mode	C0	C1	C2
Input-Split			X
Compound-Split		X	
FEV	X		X

The schematization of any PSU as a four-port device is always valid, regardless of the actual PSU constructive layout. This enables the exploitation of some general relationships between speeds, torques, and powers of the main PSU external ports which can be applied to any PS-CVT [33,35,36]. On the other hand, the PGs and OGs constructive parameters and their arrangement within the PSU lead to the definition of the basic functional parameters which rule the equations of the unified parametric model considered in this article. The constructive parameter here used for the definition of the planetary gear sets is the Willis' ratio Ψ, defined as the ratio between the rotational speed of the ring gear and the one of the sun gear while the carrier is still. The Willis' ratios of the two PGs are $\Psi_1 = -0.535$ and

$\Psi_2 = -0.481$, the fixed-ratio of the final drive is $k_{fd} = 0.379$. The functional parameters of the Voltec input-split and compound-split modes were identified in [34]. These are the mechanical points $\tau_{\#i}$ and $\tau_{\#o}$ and the corresponding speed ratios $\tau_{o\#i}$ and $\tau_{i\#o}$, listed in Table 2. The former are defined as the overall speed ratio $\tau = \omega_{out}/\omega_{in}$ achieved when the i or o shaft is motionless, respectively. In general terms, the corresponding speed ratio $\tau_{j\#k}$ is the j-th speed ratio $\tau_j = \omega_j/\omega_{in}$ achieved when the shaft k is motionless. The mechanical points often coincide with the overall speed ratio at which a mode shift occurs, since one of the two electric machines can be turned off. Therefore, a parallel hybrid functioning is achieved at the mechanical points.

Table 2. Basic functional parameters of Voltec derived in [34].

Mode	$\tau_{\#i}$	$\tau_{\#o}$	$\tau_{o\#i}$	$\tau_{i\#o}$
Input-Split	0.247	0	2.00	−1.87
Compound-Split	0.247	0.510	2.00	2.00

Once known the parameters of Table 2, the dimensionless approach addressed in [35,36] can be applied to the Voltec to analyze both the power-split and FEV operation in terms of speed, torque, and power ratios, by including the evaluation of the PSU mechanical power losses.

2.1. Dimensionless Speeds, Powers and Mechanical Losses in Voltec Power-Split Operation

The Voltec PS-CVT in power-split operation was previously analyzed in [34,35]. To avoid repetition, this section includes only the outcomes of these previous applications, not the procedure implemented to obtain them. The results are shown in Figure 2. Starting from the functional parameters of Table 2, the speed ratio $\tau_i = \omega_i/\omega_{in}$ between MG I and the ICE was computed as a function of the overall speed ratio τ, as well as the speed ratio $\tau_o = \omega_o/\omega_{in}$ between MG O and the ICE. These are shown in Figure 2a for both input- and compound-split mode. The shift between one mode to the other occurs at the mechanical point $\tau = \tau_{\#i} = 0.247$. For $\tau = \tau_* = 0.379$ both electric machines rotate at the same speed, therefore both PGs work at their synchronous condition. At the PGs synchronism, the PSU mechanical power losses (Figure 2b) show a minimum, because the absence of relative motion between PGs branches eliminates the PGs friction losses. The mechanical power losses of Figure 2b were calculated as a fraction of the input power as a function of the overall speed ratio τ and the opposite of the overall power ratio $\eta = -P_{out}/P_{in}$. Note that η is not a global efficiency, but a variable exploited to model the possibility of the battery to provide or absorb power. Therefore, it can also be far higher than one, if the demanded output power is mainly provided by the battery rather than the ICE. The PSU losses enabled the calculation of the real power that the electric machines should provide to or collect from the PSU as a fraction of the input power (Figure 2c,d).

2.2. Dimensionless Speeds, Powers and Mechanical Losses in Voltec Full-Electric Operation

The relationships exploited in [34,35] to analyze the power-split operation were rearranged in [36] to model also the FEV functioning mode. These are exploited in this section to apply the unified parametric model to the Voltec in FEV operation for the first time. Nonetheless, to find the best balance between brevity and self-consistency of the paper, this section presents the only implementation of formulas that were introduced and explained in the previous works [33–36], to which we refer the reader for more information. However, Appendix A outlines the major features of the model to facilitate the understanding of the content of this section.

As the engine is inactive in FEV driving (clutch C0 is engaged), speeds and power can be more conveniently normalized to the output ones. Since the shaft *in* is motionless, the speed ratio between every electric machine and the shaft *out* is univocally defined as:

$$\begin{aligned} \left.\frac{\omega_i}{\omega_{out}}\right|_{\omega_{in}=0} &= \frac{\tau_{i_{\#o}}}{\tau_{\#o}-\tau_{\#i}} = 7.58 \\ \left.\frac{\omega_o}{\omega_{out}}\right|_{\omega_{in}=0} &= \frac{\tau_{o_{\#i}}}{\tau_{\#i}-\tau_{\#o}} = 8.12 \end{aligned} \tag{1}$$

The functional parameters used in Equation (1) are those related to the input-split mode, since it is the only mode exploited by General Motors to perform the FEV operation.

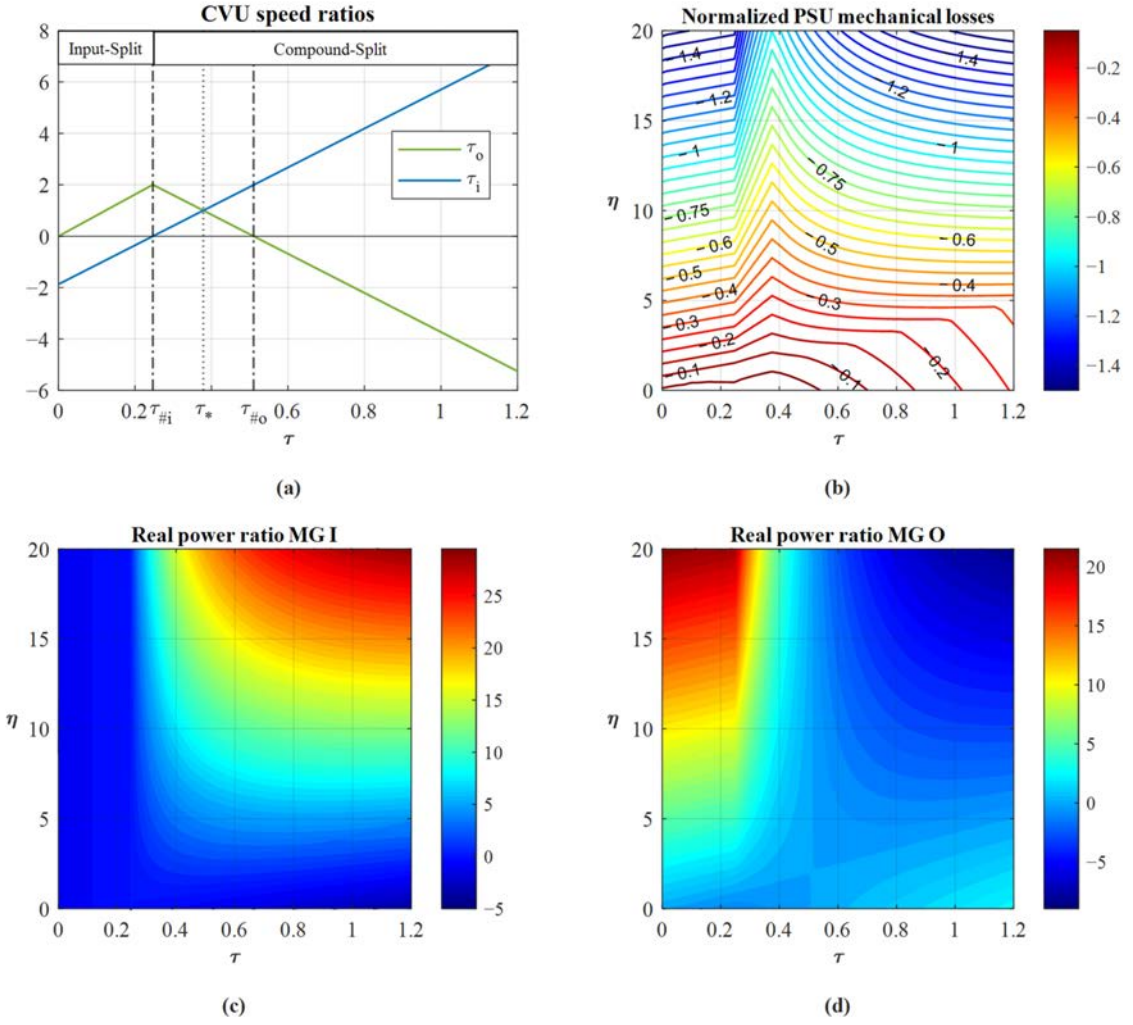

Figure 2. Results of Voltec analysis in power-split operation carried out in [34,35]. (**a**) CVU speed ratios; (**b**) mechanical power losses in the PSU as a fraction of the input power; (**c**) MG I real power as a fraction of the input power; (**d**) MG O real power as a fraction of the input power.

The dimensionless PSU power losses can be computed by the fast black-box method proposed in [35] adapted to the FEV analysis, as described in [36] and summarized in Appendix A. The considered efficiencies of the final drive ($\eta_{fd} = 0.953$) and of the PGs in fixed-carrier functioning ($\eta_0 = 0.96$) are the same as those assumed in [35]. The total mechanical power losses are the sum of those occurring in the final drive, calculated as:

$$\overline{p}'_L\big|_{OG} = -\frac{\overline{P}_{Loss}\big|_{OG}}{P_{out}} \approx -\left|\left(1-\eta_{fd}\right)\, p'_{out}\right| \tag{2}$$

and those occurring in the PGs:

$$\overline{p}'_L|_{PG1} = -\frac{\overline{P}_{Loss}|_{PG1}}{P_{out}} \approx -\left|\left(1-\eta^R\right)\left(\frac{\phi^{in}_{out/i}-\psi^R_{C/S}}{1-\psi^R_{C/S}}\right)p'_{out,1}\right| \quad (3)$$

$$\overline{p}'_L|_{PG2} = -\frac{\overline{P}_{Loss}|_{PG2}}{P_{out}} \approx -\left|\left(1-\eta^C\right)\left(\frac{\phi^{out}_{o/i}-\psi^C_{S/R}}{1-\psi^C_{S/R}}\right)p'_o\right| \quad (4)$$

The parameters used in Equations (3) and (4) are indicated in Table 3, while in Equation (3) $p'_{out,1}$ is the portion of p'_{out} flowing in PG1, which can be computed as the difference between the power flowing into the final drive (p'_{out}/η_{fd}) and its portion flowing in PG2 ($p'_{out,2}$, see Equation (A4) in Appendix A for its calculation), as follows:

$$p'_{out,1} = \frac{p'_{out}}{\eta_{fd}} - p'_{out,2} = \frac{p'_{out}}{\eta_{fd}} + p'_o\phi^i_{o/out} \quad (5)$$

Table 3. PGs reference notation, fixed-Z speed ratios, and fixed-Z efficiency [35,36].

	$x-X$	$y-Y$	$z-Z$	$\psi^Z_{X/Y}$	η^Z
PG1	*out* – Carrier	*i* – Sun	*in* – Ring	$\psi^R_{C/S}=\frac{\Psi_1}{\Psi_1-1}$	$\eta^R=\frac{1-\Psi_1}{\eta_0-\Psi_1}$
PG2	*o* – Sun	*i* – Ring	*out* – Carrier	$\psi^C_{S/R}=\frac{1}{\Psi_2}$	$\eta^C=\eta_0$

Note that $\overline{p}'_{out} = p'_{out} = -P_{out}/P_{out} = -1$ by definition. By considering $\overline{p}'_o = p'_o = -P_o/P_{out}$ as the independent variable, the total power losses $\overline{p}'_L$ can be swiftly computed by summing Equations (2)–(4). The dimensionless power flowing in the other electric machines can be calculated by the PSU real power balance:

$$\overline{p}'_o + \overline{p}'_i + \overline{p}'_L = 1 \quad (6)$$

The results of the dimensionless analysis to FEV operation are shown in Figure 3.

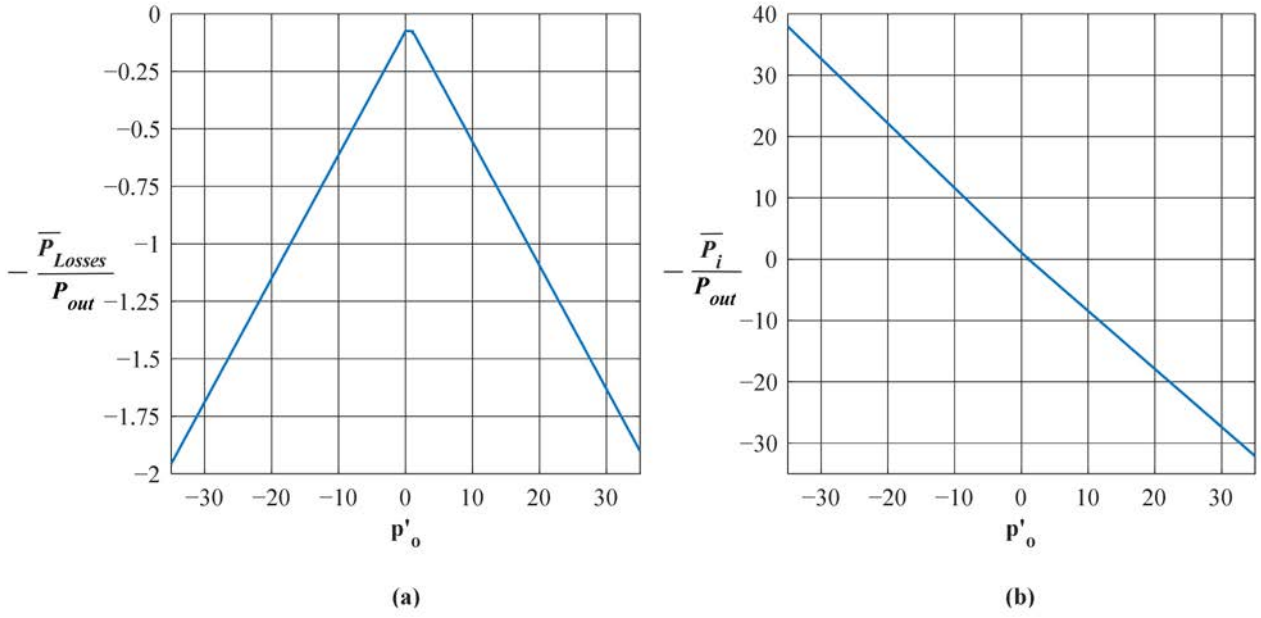

Figure 3. Results of Voltec analysis in FEV operation. (**a**) Mechanical power losses in the PSU as a fraction of $-P_{out}$; (**b**) MG I real power as a fraction of $-P_{out}$.

3. Identification of the Optimal Operating Maps

To carry out the analysis addressed in Section 2, it is sufficient to know only the constructive and functional layout of the PS-CVT. This allows the calculation of the PSU speed ratios as well as the dimensionless mechanical power that electric machines should provide or absorb, by considering the PSU friction losses. More specifically, in power-split operation, the dependent variables, which are normalized to ICE speed or power, can be assessed by freely assigning the speed ratio and the power ratio between the output and the input port (Figure 2). On the other hand, in FEV operation, the speed ratios are univocally defined, thus the dependent variables, which are normalized to the output power, can be determined by freely supposing the power ratio between one PSU port connected to an electric machine and the output port (Figure 3). In other words, for a given vehicle speed (directly related to ω_{out}) and for a given demanded torque, it is necessary to assume a specific functioning point of the ICE (in PS operation) or of one electric machine (in FEV operation) to univocally determine speeds and powers (and thus torques) on each PSU port.

Obviously, the output torque and the wheels' speed can be considered independently one from the other, but if the output torque is higher or lower than the driving resistance, the powertrain work in dynamic operations, and the inertia of the vehicle and the propulsors should be considered in the analysis. In this article, for computational simplicity, the steady-state operation is analyzed, whereby the output torque is a function of the vehicle speed (V_{veh}), thus the power delivered by the powertrain is:

$$P_{out} = -\left(mg\sin\alpha + f_r mg\cos\alpha + 0.5 \cdot C_d A_f \rho_a V_{veh}^2\right) V_{veh} \quad (7)$$

where m, f_r, C_d, A_f are the Chevrolet Volt parameters reported in Table 4, α is the road slope in radians, $g = 9.81\ m/s^2$ is the gravitational acceleration, and $\rho_a = 1.225\ kg/m^3$ is the air density. It is worth noting that m is the sum of the unladen vehicle mass m_0 and the mass of passengers, fuel, or any other additional load. Therefore, m and α depend on the driving conditions. Nonetheless, it is sufficient to modify these values upstream of the procedure described in this section so as to obtain data referred to any steady-state driving condition.

Table 4. Chevrolet Volt parameters.

Unladen Mass m_0 [kg]	Rolling Resistance f_r	Drag Coefficient C_d	Frontal Area A_f [m^2]	Wheel Radius R_w [m]
1603	0.0113	0.28	2.20	0.323

Once fixed a vehicle speed, the functioning point of the ICE in power-split operation or of one electric machine in FEV operation has to be selected so as to determine $\tau = V_{veh}/(R_w \cdot \omega_{in})$ and $\eta = -P_{out}/P_{in}$, or $p'_o = -P_o/P_{out}$, respectively. To investigate all the viable powertrain functioning points for given vehicle speed, the whole range of operation of the ICE or MG O has to be explored. Therefore, the efficiency maps of the propulsors are needed (Figures 4 and 5). These are necessary also for evaluating the propulsors efficiency in each achievable working point.

3.1. Calculation of Optimal Operating Maps in Power-Split Operations

For a given vehicle speed V_{veh} and subsequent output power P_{out}, the powertrain operation can be analyzed by considering each couple of ICE speed and torque (ω_{in}, T_{in}) ranging from their minimum and maximum values within the ICE operation range of Figure 4. This leads to the calculation of an overall speed ratio matrix, having the same dimension of the ICE efficiency map, where each element is $\tau = V_{veh}/(R_w \cdot \omega_{in})$. A corresponding overall power ratio matrix containing $\eta = -P_{out}/(\omega_{in} \cdot T_{in})$ can be obtained, too. Hence, these matrices can be used to interpolate the dimensionless results of Figure 2, in

order to identify the speed and power ratios of the electric machines for each combination of τ and η. Then, these ratios can be multiplied by the corresponding ω_{in} and P_{in} to assess the dimensional rotational speed of the electric machines (ω_i, ω_o) and their mechanical power ($\overline{P}_i$, $\overline{P}_o$). In this way, the operating point of both electric machines is univocally determined, as is their efficiency which enables the calculation of the net electric power flowing to or from the battery as follows:

$$P_{batt}(V_{veh}, \omega_{in}, T_{in}) = \overline{P}_i \eta_I^{-sign(\overline{P}_i)} + \overline{P}_o \eta_O^{-sign(\overline{P}_o)} \quad (8)$$

The positive sign of the power flows is shown in Figure 1.

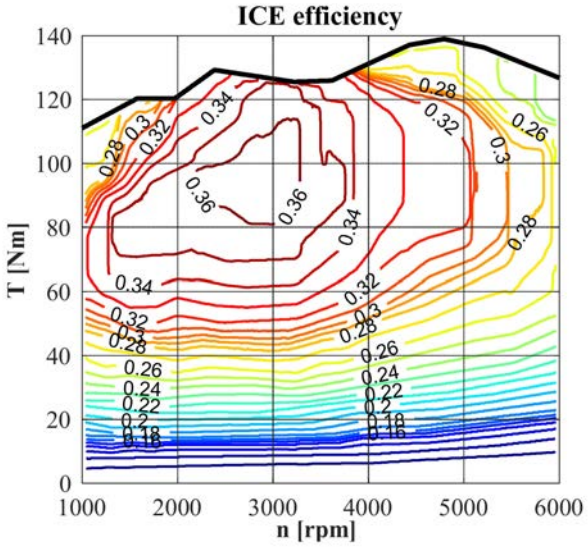

Figure 4. Efficiency map of the Chevrolet Volt ICE derived from [37].

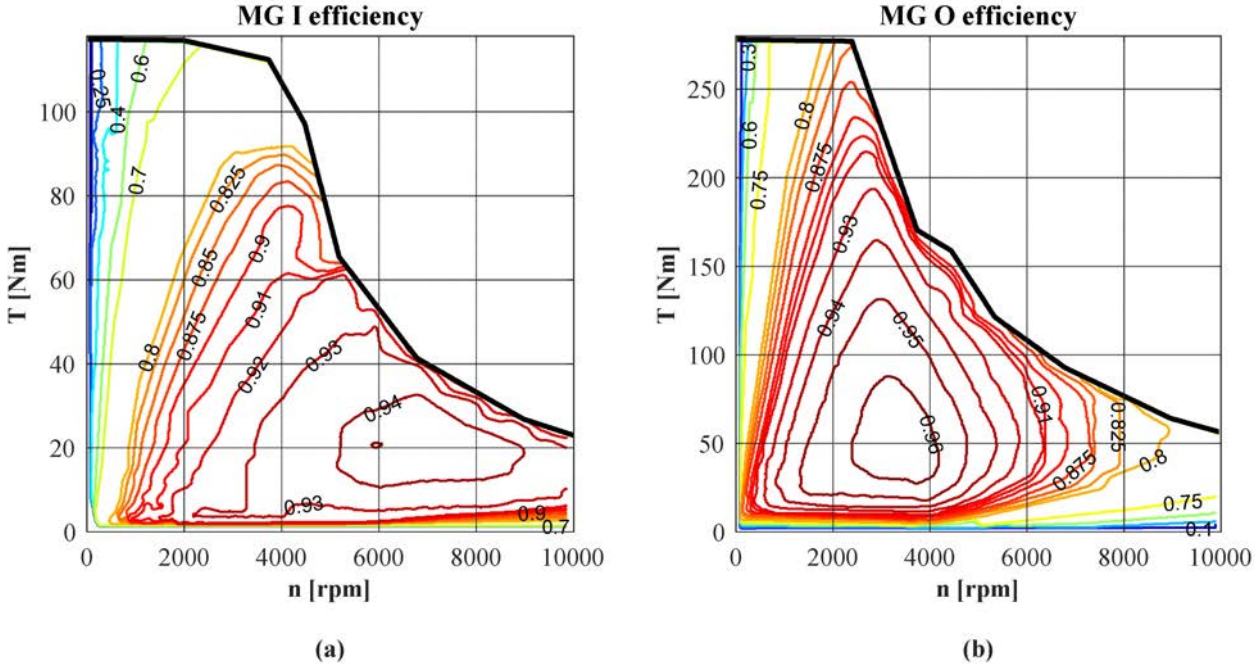

Figure 5. Efficiency maps of Chevrolet Volt electric machines derived from [38]; (**a**) Motor Generator I; (**b**) Motor Generator O. Exploited for both motoring and generating operation.

Hence, by the simple procedure herein addressed, it is possible to obtain a set of matrices containing all data describing the powertrain steady-state operation, which can be exploited as a basis of the desired energy management strategy. As an example, in this paper, a procedure for pursuing maximum global efficiency is proposed. According to the direction of the battery power, P_{batt} can be an output or input power in the powertrain. Therefore, if $P_{batt} > 0$ the battery supports the ICE in the vehicle propulsion, and the global efficiency is:

$$\eta_{gl}(V_{veh}, \omega_{in}, T_{in}) = -\frac{P_{out}}{P_{fuel} + P_{batt}} \quad (9)$$

where $P_{fuel} = P_{in}/\eta_{ICE}$ is the power provided by fuel combustion. η_{ICE} can be derived for each combination of ω_{in} and T_{in} from Figure 4. If $P_{batt} < 0$ the ICE delivers power in surplus which can be used to recharge the battery, and the global efficiency is:

$$\eta_{gl}(V_{veh}, \omega_{in}, T_{in}) = -\frac{P_{out} + P_{batt}}{P_{fuel}} \quad (10)$$

Eventually, it is possible to extract the maximum value from the matrix η_{gl} for a given vehicle speed and find the related ICE and electric machines operation resulting in the most efficient driving.

Nevertheless, the working points which violate a constructive constraint of propulsors, power converters, or batteries should not be included among the potential optimal ones. Therefore, the final operating maps do not include the functioning points whereby the ICE or electric machines operation is not included within the maps of Figures 4 and 5, or the electric powers overcome their respective maximum limits of power converters or batteries (Table 5).

Table 5. Maximum power of battery and power converters of Chevrolet Volt derived from [37,39].

Power Converter I Max. Power [kW]	Power Converter O Max. Power [kW]	Battery Pack Max. Power [kW]
48	87	120

In fact, the real constraint on P_{batt} depends on the battery state of charge (SOC):

$$P_{max\_charge}(\text{SOC}) \leq P_{batt} \leq P_{max\_discharge}(\text{SOC}) \quad (11)$$

P_{max_charge} and $P_{max\_discharge}$ should be evaluated instantaneously by a deeper dynamic analysis. However, a simplified approach is exploited in the following to swiftly analyze four different scenarios, summarized in Table 6:

- SOC comprised between its lower and higher thresholds (SOC = FREE);
- Battery completely discharged (SOC = 0);
- Battery completely charged (SOC = 1);
- Maintaining-charge driving (SOC = CONSTANT).

Table 6. Adjusted constraints on battery power according to the SOC.

SOC	P_{max_charge} [kW]	$P_{max\_discharge}$ [kW]
FREE	−120	120
0	−120	0
1	0	120
CONSTANT	0	0

3.2. Calculation of Optimal Operating Maps in FEV Operations

For given vehicle speed, in FEV driving the rotational speeds of the electric machines are univocally determined by Equation (1), therefore the only degree of freedom is the

torque of one electric machine. As stated in Section 2, by choosing as the independent variable the torque of MG O, which can range from its minimum to maximum value corresponding to each rotational speed (Figure 5), it is possible to consider an array with different values of $p'_o = -(\omega_o \cdot T_o)/P_{out}$. This can be used to interpolate the dimensionless results of Figure 3b and find the potential operating points of MG I for given P_o and P_{out}. Then, similarly to Section 3.1, P_{batt} can be calculated by Equation (8) and the global efficiency in FEV operation is simply:

$$\eta_{gl}(V_{veh}, T_o) = -\frac{P_{out}}{P_{batt}} \tag{12}$$

In FEV operation, the battery SOC is supposed to be always sufficient to provide the demanded power.

4. Results and Discussion

The procedure described in Section 3 for calculating the optimal operating maps was implemented in MATLAB, after having carried out the dimensionless approach reported in Section 2. The following results were computed by considering a total vehicle mass equal to $m = 1750$ kg in plain ($\alpha = 0$ rad). The analyzed vehicle speed ranges from 5 to 200 km/h.

4.1. Results in Power-Split Operations

The mesh grid used in input to the script was obtained by the arrays $\omega_{in} = 1000 : 10 : 6000$ rpm and $T_{in} = 10 : 1 : 140$ Nm. The procedure described in Section 3.1 was carried out for each vehicle speed, whereby the respective optimal operating point was selected after excluding those outside the boundaries of Figures 4 and 5, Table 5, Equation (11), and Table 6. The results of Figures 6–11 show the optimal operating points resulting from the optimization procedure aimed at minimizing the powertrain power losses.

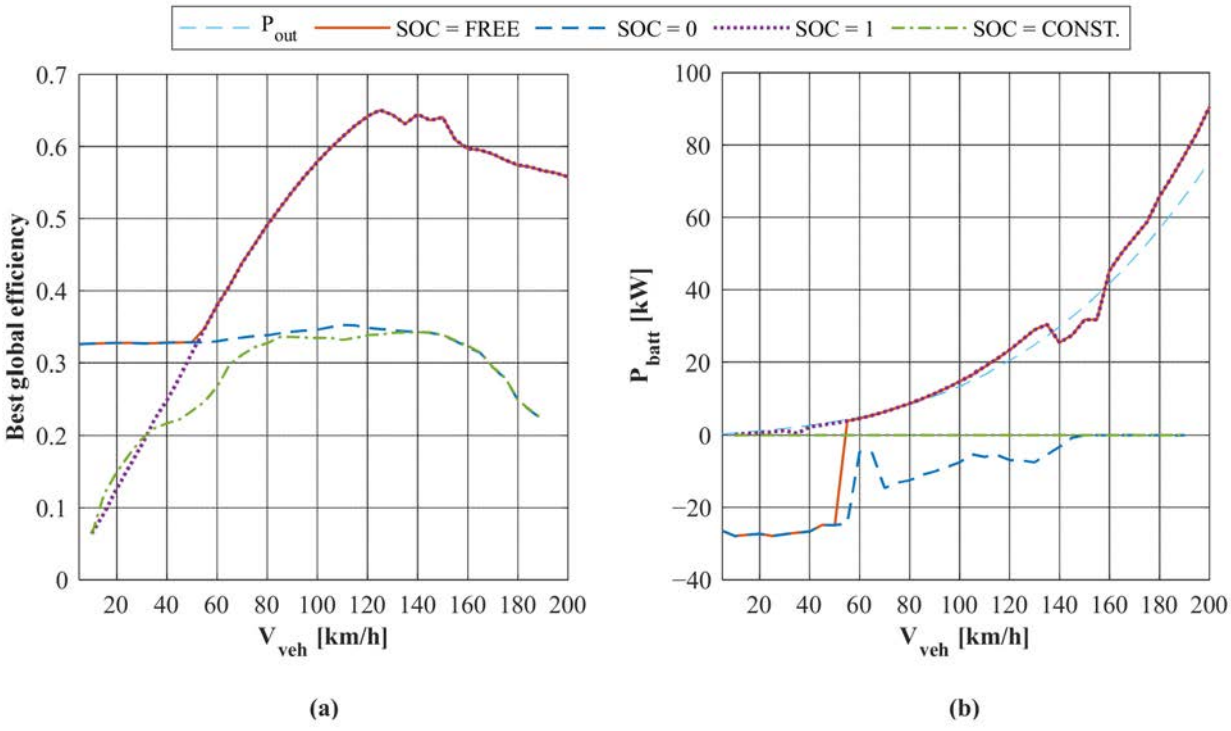

Figure 6. (**a**) Best global efficiency in power-split operation; (**b**) battery power in the optimal power-split operating points.

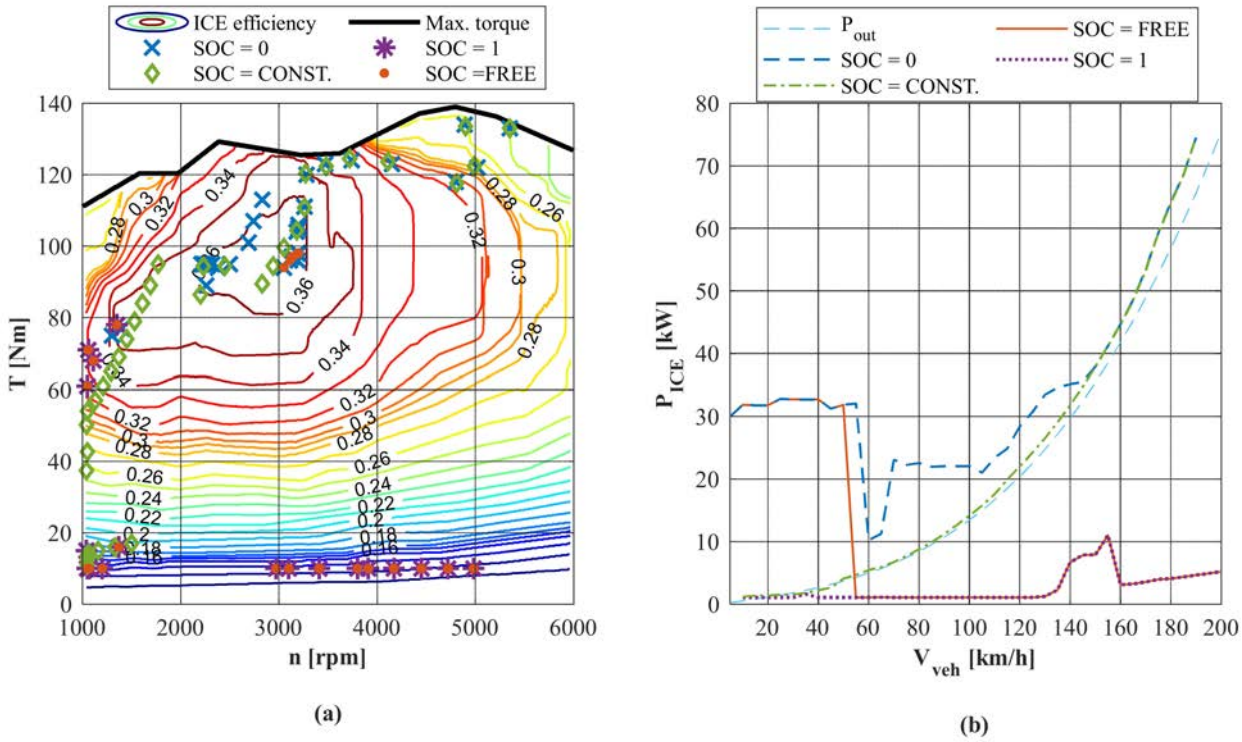

Figure 7. ICE optimal power-split operation: (**a**) ICE functioning points; (**b**) ICE power.

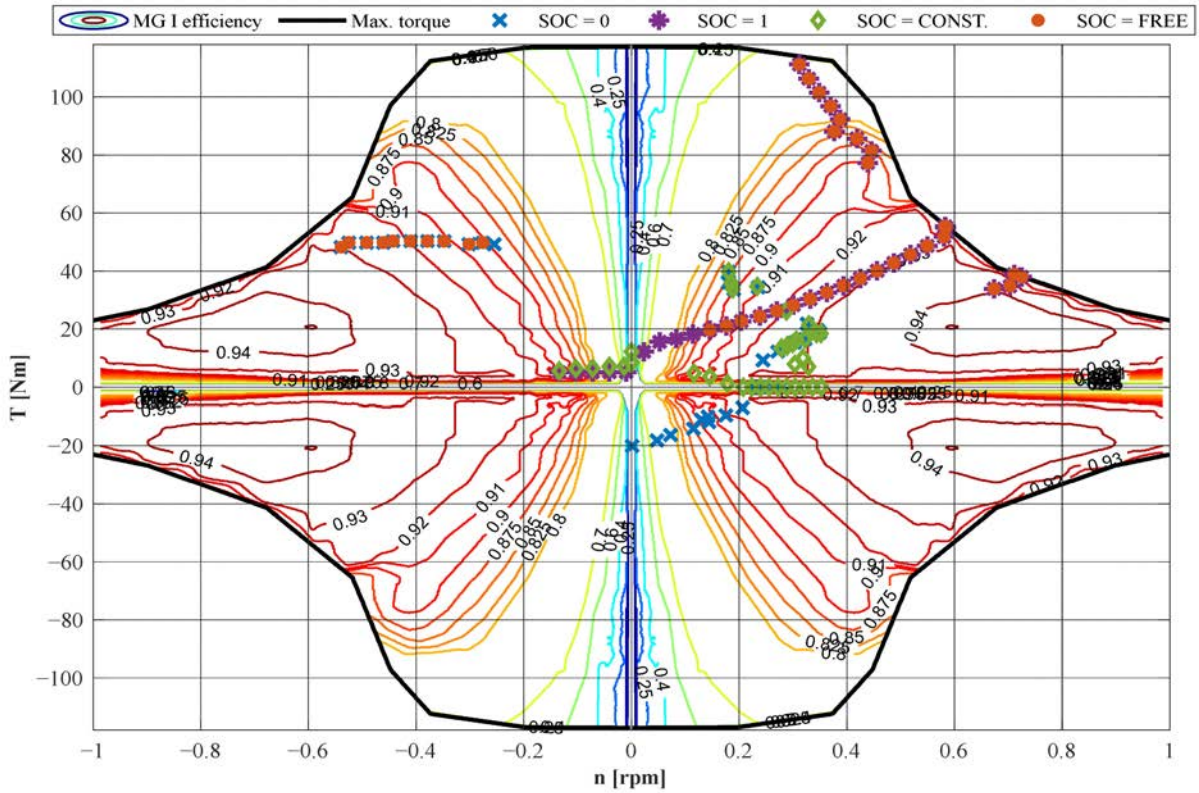

Figure 8. MG I optimal functioning points in power-split operation.

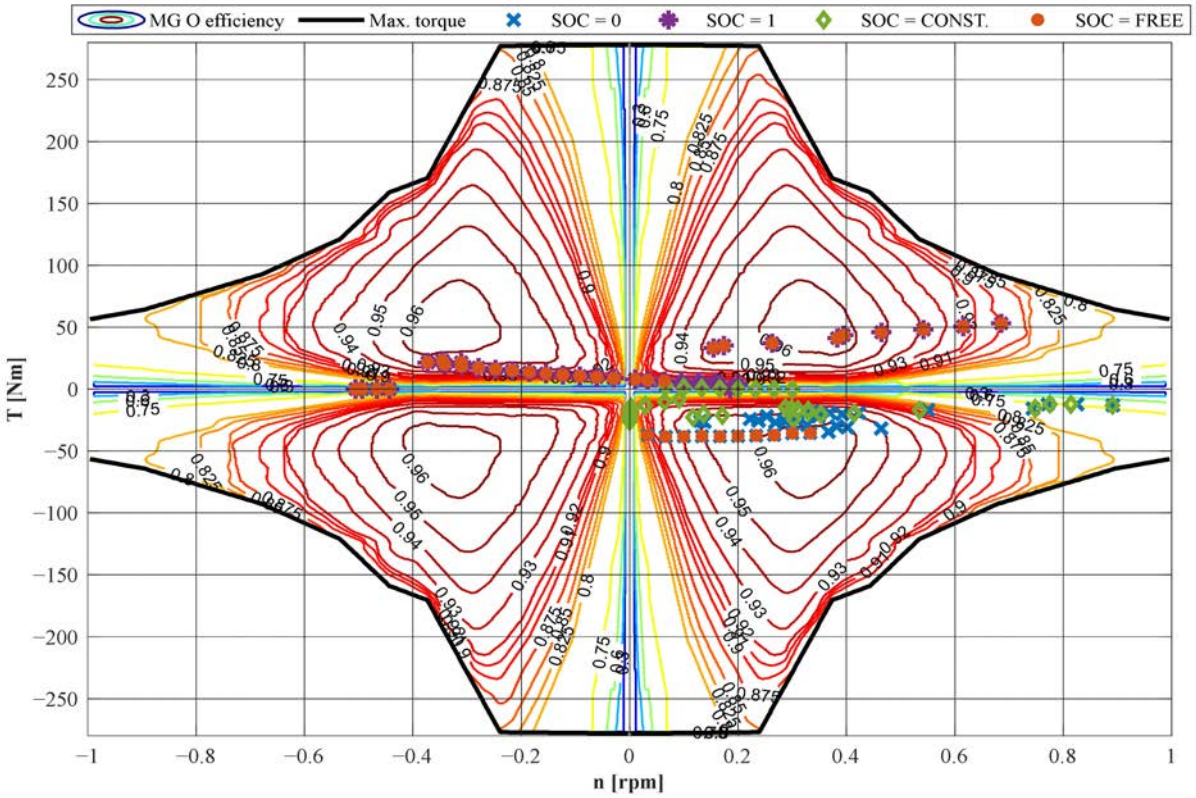

Figure 9. MG O optimal functioning points in power-split operation.

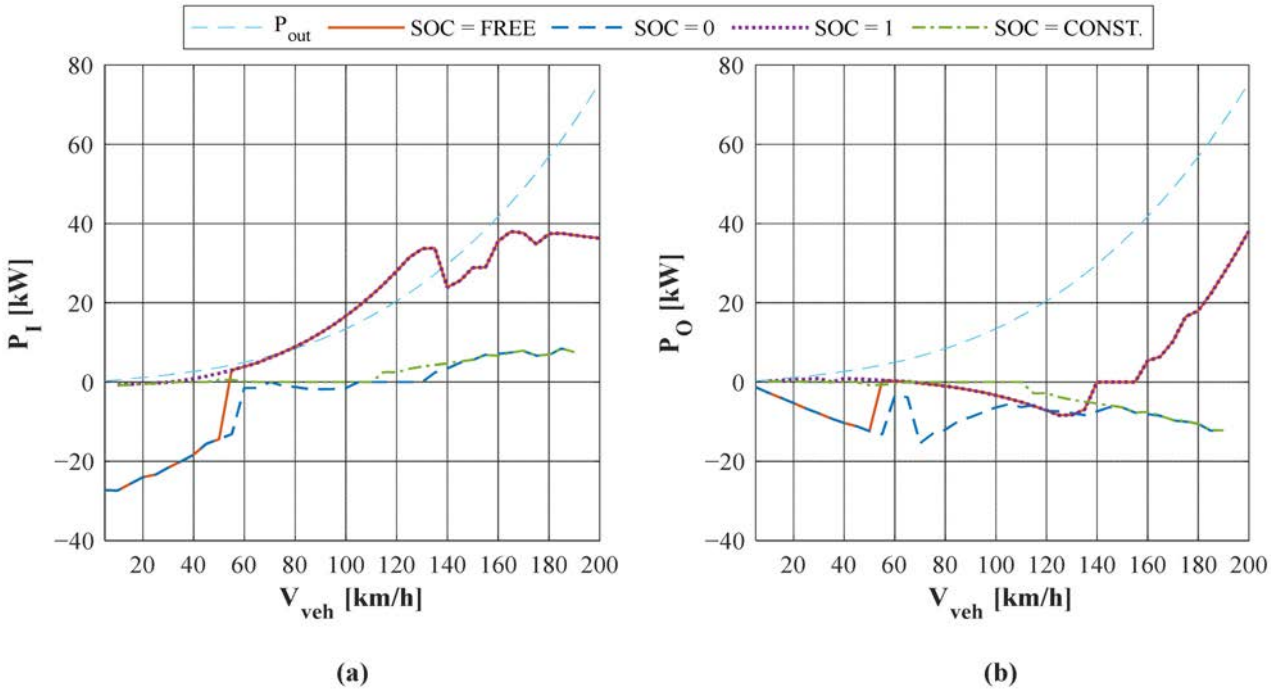

Figure 10. Electric machines optimal power in power-split operation: (**a**) MG I power; (**b**) MG O power.

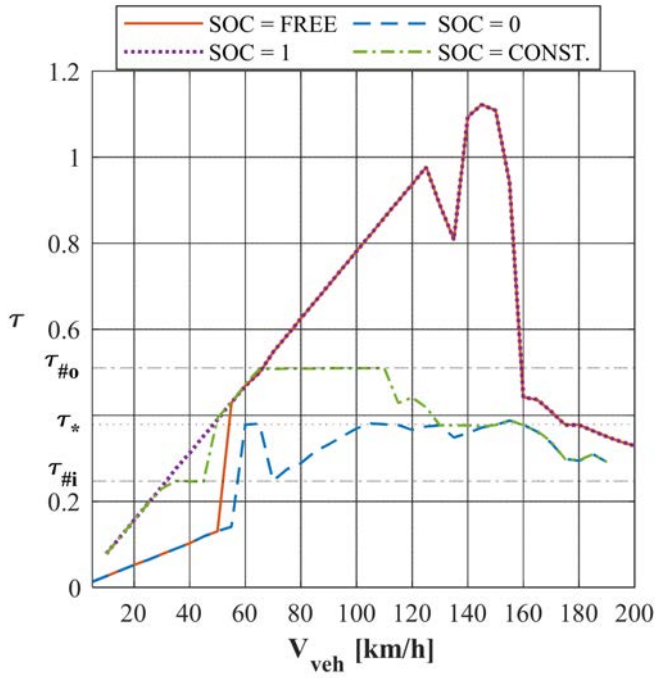

Figure 11. Optimal overall transmission ratio and mode selection in power-split operation.

Figure 6a shows that the best results are achieved for SOC = FREE since the availability of the battery both as a power source and power storage would enable the achievement of the most efficient power flows (Figure 10). Nevertheless, the maximum global efficiency is lower than 0.33 up to 50 km/h, therefore it would be more advisable to turn off the engine and drive in FEV operation (see Section 4.2). The only reason to let the ICE work at lower speeds is to recharge the battery if possible (SOC = FREE or SOC = 0). In this case, the ICE should operate in the maximum efficiency region, otherwise, it should be turned off also for higher speeds if the battery can supply power for propulsion (SOC = FREE or SOC = 1) (Figure 7). In this way, the global efficiency would be significantly enhanced (Figure 6a), since the demanded output power would be provided by the electric unit (Figure 6b), which is more efficient than the ICE.

Nevertheless, a more robust control strategy should regulate the battery power according to the instantaneous SOC, so as to ensure sufficient range. Indeed, for speeds higher than 100 km/h, the optimal powertrain operation would be achieved at the expense of the driving range. Therefore, over 100 km/h would be even more advisable to limit the power supplied by the battery and increase that provided by the ICE, even though this would reduce the global efficiency.

On the other hand, if the battery is completely discharged (SOC = 0) or a maintaining-charge driving is desired (SOC = CONSTANT), the demanded output power should be provided mainly by the engine (Figure 7b). In this case, the battery charging would be recommended between 50 and 145 km/h, while over 145 km/h keeping the SOC constant would result in greater efficiency. Nonetheless, since the ICE maximum power is 75 kW [37], the vehicle speed cannot exceed 190 km/h with SOC = 0 or SOC = CONSTANT.

Figures 8–10 show the optimal exploitation of the electric machines in power-split operation. They suggest using both MG I and MG O as generators for battery recharging up to 50 km/h. It should be the same from 50 to 130 km/h if SOC = 0, while MG I should be used as a motor and MG O as a generator if the battery can provide power (SOC = FREE or SOC = 1). In the latter case, the mechanical energy converted to electric energy by MG O is reconverted to the mechanical form by MG I. Over 155 km/h, both MG I and MG O should be used as motors for SOC = FREE or SOC = 1.

To assess the optimal mode selection, it is sufficient to analyze the optimal overall transmission ratio of Figure 11.

Figure 11 shows that for lower speeds the input-split mode should be preferred, while the compound-split mode is advisable at higher speeds. Moreover, it is worth noting that for SOC = 0 and SOC = CONSTANT (i.e., if the battery cannot provide power for propulsion) the optimal overall speed ratio at medium-high speed is the one that realizes the PGs synchronism, where the mechanical power losses are minimized (Figure 2).

4.2. Results in FEV Operations

The array used in input to the script was $T_o = -280 : 1 : 280$ Nm. The procedure described in Section 3.1 was carried out for each vehicle speed, whereby the respective optimal operating point was selected after excluding those outside the boundaries of Figure 5 and Table 5. The results of Figures 12 and 13 are related to the best powertrain operating points resulting in the highest global efficiency for each vehicle speed.

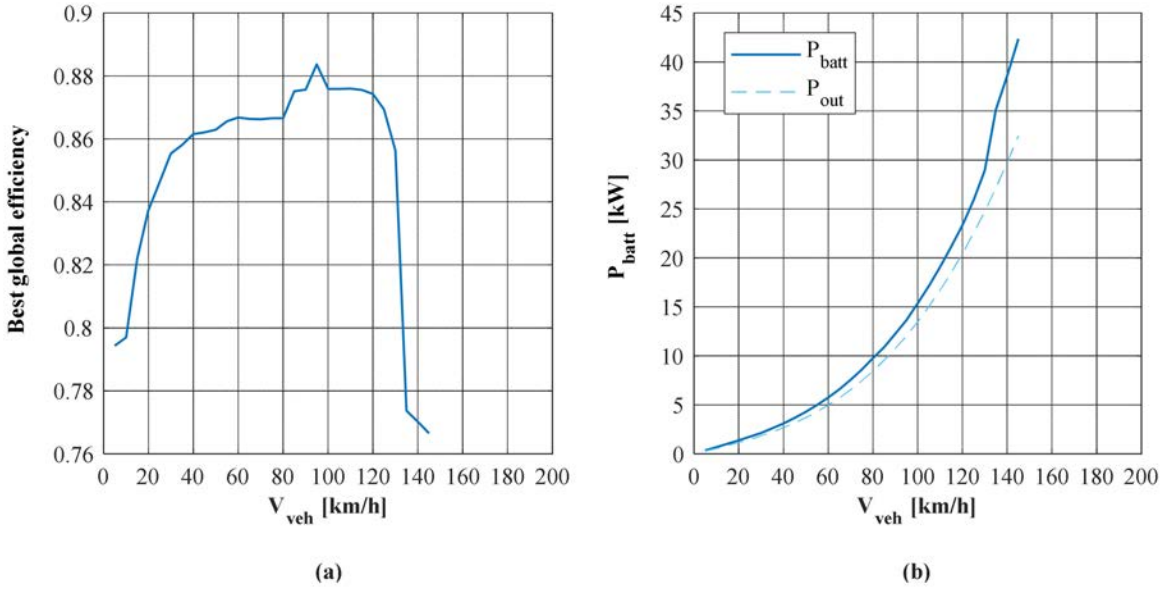

Figure 12. (**a**) Best global efficiency in FEV operation; (**b**) battery power in the optimal FEV operating points.

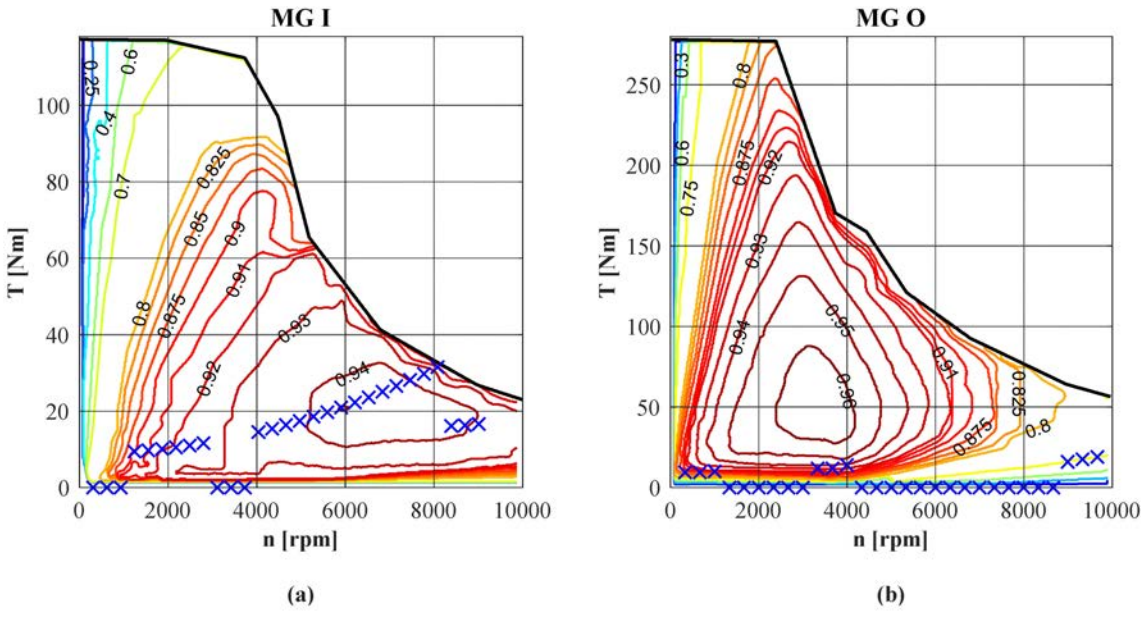

Figure 13. Electric machines optimal FEV operation, indicated by "X": (**a**) MG I functioning points; (**b**) MG O functioning points.

Figure 12a shows that the global efficiency in FEV operation is averagely higher than the one achievable in power-split operation, thus the FEV driving is specifically suggested for low–medium speed. As stated in Section 4.1, exploiting the only battery power for propelling the vehicle in steady-state driving at higher speeds would imply a reduced range, thus it should be avoided. Over 145 km/h the FEV driving cannot be realized because the required rotational speed of MG O would overcome its maximum value. Figure 13 shows that the optimal FEV operation in steady-state driving involves the exploitation of MG I except for two limited vehicle ranges from 5 to 15 km/h and from 50 to 60 km/h. From 135 to 145 it is advisable to operate with both electric machines acting as motors.

5. Conclusions

This article is an advancement of the previous contributions [33–36] addressing a unified parametric model for the analysis of PS-CVT. Herein it was applied to the Chevrolet Volt by introducing the propulsors efficiency maps to move from a dimensionless approach to a dimensional one. The final aim was to provide a complete and general tool to comprehensively analyze any power-split transmission, even multi-PG and multi-mode as Voltec is, by assessing also the mechanical power losses which are often neglected owing to the difficulty of their calculation. The FEV operation can also be swiftly analyzed.

As described in Sections 3 and 4, this method enables the investigation of the powertrain response for given vehicle speed and demanded torque. All the viable operating points are available as a set of operating maps containing the propulsors functioning points, their efficiency, the mechanical power losses in the transmission, the battery power, and the global efficiency. These data can be exploited for the development of the desired energy management strategy.

As an example, far from presenting it as an exhaustive control strategy, this paper proposes a procedure for selecting the optimal operating points which maximize the powertrain global efficiency in steady-state power-split and FEV driving. The results showed the importance of properly handling the batteries SOC to ensure the possibility of exploiting them as an energy exchanger, as well as the benefit of PGs synchronism to reduce the friction losses. Nonetheless, it seems that the MG O appears to be under-exploited in steady-state driving (Figure 9). This can be due to the fact that the surplus power of MG O could be used to provide an acceleration boost, thus it might be exploited more in dynamic operation, which was not analyzed here.

Therefore, future research could be aimed at extending the model in this very direction. Indeed, its basic relationships between PSU speed, torque, and power ratios proposed in [33,35,36] would be still valid in dynamic operation, being based on the principle of power conservation. However, the correspondence between torques developed at the PSU main ports and those provided by the propulsors would be missing because of inertial effects caused by acceleration or deceleration of the vehicle and the propulsors themselves. The extension of the model to the dynamic condition would enable a more in-depth simulation of the powertrain operation which could instantaneously consider the actual battery SOC or the power converters' efficiency. After collecting the results of this sort of simulation, they can be used to develop the most robust energy management strategies available in the literature to optimize the desired objective function, which can be even the minimization of the mechanical power losses.

Author Contributions: Methodology, M.C.; Software, A.C.; Supervision, M.C.; Writing—original draft, A.C.; Writing—review & editing, A.C. and M.C. All authors have read and agreed to the published version of the manuscript.

Funding: This research received no external funding.

Institutional Review Board Statement: Not applicable.

Informed Consent Statement: Not applicable.

Data Availability Statement: Not applicable.

Conflicts of Interest: The authors declare no conflict of interest.

Nomenclature

k_x	Fixed-gear ratio on the x-th branch
P_j or $\overline{P}_j$	Ideal or real power in the j-th branch
p_j or $\overline{p}_j$	Dimensionless ideal or real power in the j-th branch as a fraction of the input power
p'_j or $\overline{p}'_j$	Dimensionless ideal or real power in the j-th branch as a fraction of the output power
$\overline{P}_{Loss}$	Mechanical power losses
$\overline{p}_L$	Dimensionless mechanical power losses as a fraction of the input power
$\overline{p}'_L$	Dimensionless mechanical power losses as a fraction of the output power
T_j	Torque applied to the j-th shaft
η	Opposite of the overall power ratio ($\eta = -P_{out}/P_{in}$)
η_0	Fixed-carrier efficiency of a PG
η^Z	Fixed-Z apparent efficiency of a PG
η_{gl}	Powertrain global efficiency
η_I and η_O	Efficiency of the electric machines I and O
η_{ICE}	Efficiency of the internal combustion engine
$\eta_{X/x}$	Efficiency of the x-th OG
τ	Overall speed ratio
τ_j	Speed ratio of the j-th shaft
$\tau_{\#j}$	Overall speed ratio for which the j-th shaft is motionless (i.e., mechanical point or nodal ratio)
$\tau_{j\#k}$	Speed ratio of the j-th shaft when the k-th shaft is motionless (i.e., corresponding speed ratio)
τ_*	Overall speed ratio for which one or more PGs work at synchronism
$\phi^z_{x/y}$	Generalized characteristic function
Ψ	Willis' ratio of a PG
$\psi^Z_{Y/X}$	Fixed-Z speed ratio of a PG
ω_j	Rotational speed of the j-th shaft

Appendix A

The basic theory of the unified parametric model addressed in this paper considers the PSU made up of one or more three-port mechanisms (TPMs), which consists of one active PG and up to three OGs (Figure A1). X, Y, Z indicate a general way to refer to the PG branches (ring gear, sun gear, and carrier); x, y, z indicate a general way to refer to the PSU main port (*in*, *out*, *i*, *o*).

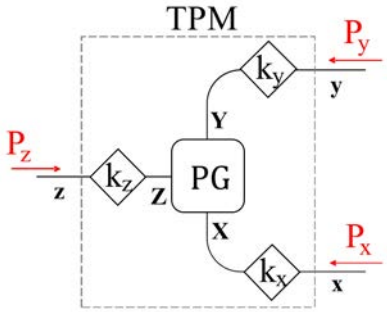

Figure A1. Scheme of a three-port mechanism with one PG (illustrated by a rounded-corner square) and three OGs (rhombi) realizing the k_j fixed-ratio. Red arrows indicate the positive direction of power flows.

The nomenclature adopted in this model distinguishes between torques and powers assessed by considering the PSU ideal or real. In the latter case, torques and powers symbols are overlined. Nonetheless, this distinction affects only the dependent variables, which are supposed to counterbalance the PSU mechanical power losses. Moreover, capital

letters indicate dimensional power flows, while the dimensionless ones are indicated by lowercase letters without or with an apex, depending on whether they are normalized to the input power (P_{in}) or to the opposite of the output power ($-P_{out}$), respectively. The former normalization is exploited to address power-split operation, while the latter is used in FEV analysis.

The total mechanical power losses ($\overline{p}'_L$ in FEV operation) are the sum of the losses occurring in OGs and PGs, which can be derived as follows:

$$\overline{p}'_L\big|_{OG} = -\frac{\overline{P}_{Loss}\big|_{OG}}{P_{out}} \approx -\left|\left(1-\eta_{X/x}\right) p'_x\right| \tag{A1}$$

$$\overline{p}'_L\big|_{PG} = -\frac{\overline{P}_{Loss}\big|_{PG}}{P_{out}} \approx -\left|\left(1-\eta^Z\right)\left(\frac{\phi^z_{x/y}-\psi^Z_{X/Y}}{1-\psi^Z_{X/Y}}\right) p'_x\right| \tag{A2}$$

In Equation (A1) $\eta_{X/x}$ is the OG efficiency, while in Equations (A1) and (A2) $p'_x = -P_x/P_{out}$ is the normalized power ratio of the x-th shaft. In Equation (A2) η^Z is the efficiency of the PG evaluated when its branch Z is still, while $\psi^Z_{X/Y}$ is the speed ratio between branches X and Y when Z is still. Therefore, both η^Z and $\psi^Z_{X/Y}$ are constant parameters depending on the PG Willis' ratio Ψ and its basic fixed-carrier efficiency η_0 [36]. $\phi^z_{x/y}$ is the characteristic function, crucial tool for both analysis and design purpose [33,36], which is a function of τ ruled by nodal ratios:

$$\phi^z_{x/y} = \frac{\tau_x/\tau_y\big|_{\tau_z=0}}{\tau_x/\tau_y} = \frac{\tau_{\#z}-\tau_{\#x}}{\tau_{\#z}-\tau_{\#y}}\cdot\frac{\tau-\tau_{\#y}}{\tau-\tau_{\#x}} \tag{A3}$$

It is worth noting that in FEV operation $\tau \to \infty$; this can be modeled in numeric software by considering a value of τ high enough (e.g., 10^5). Moreover, the characteristic functions rule the ideal power ratio between two TPM shafts:

$$\phi^z_{x/y} = -\frac{P_y}{P_x} = -\frac{p'_y}{p'_x} \tag{A4}$$

References

1. Guzzella, L.; Sciarretta, A. *Vehicle Propulsion Systems: Introduction to Modeling and Optimization*; Springer: Berlin/Heidelberg, Germany, 2013; ISBN 9783642359132.
2. Mi, C.; Abul Masrur, M. *Hybrid Electric Vehicles, Principles and Applications with Practical Perspectives*, 2nd ed.; Wiley: Hoboken, NJ, USA, 2018; ISBN 9780470747735.
3. Krithika, V.; Subramani, C. A comprehensive review on choice of hybrid vehicles and power converters, control strategies for hybrid electric vehicles. *Int. J. Energy Res.* **2018**, *42*, 1789–1812. [CrossRef]
4. Zhuang, W.; Li, S.; Zhang, X.; Kum, D.; Song, Z.; Yin, G.; Ju, F. A survey of powertrain configuration studies on hybrid electric vehicles. *Appl. Energy* **2020**, *262*, 114553. [CrossRef]
5. Singh, K.V.; Bansal, H.O.; Singh, D. A comprehensive review on hybrid electric vehicles: Architectures and components. *J. Mod. Transp.* **2019**, *27*, 77–107. [CrossRef]
6. Zeng, X.; Wang, J. *Analysis and Design of the Power-Split Device for Hybrid Systems*, 1st ed.; Springer: New York, NY, USA, 2017; ISBN 9789811042720.
7. Chen, H.; Li, L.; Lange, A.; Küçükay, F. Innovative Dedicated Hybrid Transmission Concepts in the Next Generation of Hybrid Powertrains. *SAE Int. J. Altern. Powertrains* **2019**, *8*, 75–88. [CrossRef]
8. Sieg, C.; Küçükay, F. Benchmarking of Dedicated Hybrid Transmissions. *Vehicles* **2020**, *2*, 100–125. [CrossRef]
9. Kim, N.; Kwon, J.; Rousseau, A. Trade-off between multi-mode powertrain complexity and fuel consumption. In Proceedings of the 25th World Battery, Hybrid and Fuel Cell Electric Vehicle Symposium & Exhibition, Shenzhen, China, 5–9 November 2010.
10. Zhuang, W.; Zhang, X.; Ding, Y.; Wang, L.; Hu, X. Comparison of multi-mode hybrid powertrains with multiple planetary gears. *Appl. Energy* **2016**, *178*, 624–632. [CrossRef]
11. De Pinto, S.; Mantriota, G. Power Flows in Compound Transmissions for Hybrid Vehicles. *Machines* **2019**, *7*, 19. [CrossRef]
12. Bottiglione, F.; Mantriota, G. Power Flows and Efficiency of Output Compound e-CVT. *Int. J. Veh. Technol.* **2015**, *2015*, 136437. [CrossRef]

13. Gupta, A.K.; Ramanarayanan, C.P. Analysis of circulating power within hybrid electric vehicle transmissions. *Mech. Mach. Theory* **2013**, *64*, 131–143. [CrossRef]
14. Panday, A.; Bansal, H.O. A review of optimal energy management strategies for hybrid electric vehicle. *Int. J. Veh. Technol.* **2014**, *2014*, 160510. [CrossRef]
15. Zhang, F.; Wang, L.; Coskun, S.; Pang, H.; Cui, Y.; Xi, J. Energy management strategies for hybrid electric vehicles: Review, classification, comparison, and outlook. *Energies* **2020**, *13*, 3352. [CrossRef]
16. Zhang, P.; Yan, F.; Du, C. A comprehensive analysis of energy management strategies for hybrid electric vehicles based on bibliometrics. *Renew. Sustain. Energy Rev.* **2015**, *48*, 88–104. [CrossRef]
17. Enang, W.; Bannister, C. Modelling and control of hybrid electric vehicles (A comprehensive review). *Renew. Sustain. Energy Rev.* **2017**, *74*, 1210–1239. [CrossRef]
18. Pennestrì, E.; Mariti, L.; Valentini, P.P.; Mucino, V.H. Efficiency evaluation of gearboxes for parallel hybrid vehicles: Theory and applications. *Mech. Mach. Theory* **2012**, *49*, 157–176. [CrossRef]
19. Esmail, E.L.; Pennestrì, E.; Cirelli, M. Power-Flow and Mechanical Efficiency Computation in Two-Degrees-of-Freedom Planetary Gear Units: New Compact Formulas. *Appl. Sci.* **2021**, *11*, 5991. [CrossRef]
20. Cammalleri, M. Efficiency of split-way CVT's. A simplified model. *SAE Trans.* **2007**, *116*. [CrossRef]
21. Yang, F.; Feng, J.; Zhang, H. Power flow and efficiency analysis of multi-flow planetary gear trains. *Mech. Mach. Theory* **2015**, *92*, 86–99. [CrossRef]
22. De Carlo, M.; Mantriota, G. Electric vehicles with two motors combined via planetary gear train. *Mech. Mach. Theory* **2020**, *148*, 103789. [CrossRef]
23. Mantriota, G.; Reina, G. Dual-Motor Planetary Transmission to Improve Efficiency in Electric Vehicles. *Machines* **2021**, *9*, 58. [CrossRef]
24. Kang, J.; Choi, W.; Kim, H. Development of a control strategy based on the transmission efficiency with mechanical loss for a dual mode power split-type hybrid electric vehicle. *Int. J. Automot. Technol.* **2012**, *13*, 825–833. [CrossRef]
25. Anselma, P.G.; Biswas, A.; Belingardi, G.; Emadi, A. Rapid assessment of the fuel economy capability of parallel and series-parallel hybrid electric vehicles. *Appl. Energy* **2020**, *275*, 115319. [CrossRef]
26. Kim, N.D.; Kim, J.M.; Kim, H.S. Control strategy for a dual-mode electromechanical, infinitely variable transmission for hybrid electric vehicles. *Proc. Inst. Mech. Eng. Part D J. Automob. Eng.* **2008**, *222*, 1587–1601. [CrossRef]
27. Park, J.; Park, J.-H. Development of equivalent fuel consumption minimization strategy for hybrid electric vehicles. *Int. J. Automot. Technol.* **2012**, *13*, 835–843. [CrossRef]
28. Lee, W.; Park, J.; Kim, N. Analysis of Transmission Efficiency of a Plug-In Hybrid Vehicle Based on Operating Modes. *Int. J. Precis. Eng. Manuf.-Green Technol.* **2021**, *8*, 165–175. [CrossRef]
29. Kim, N.; Choi, S.; Jeong, J.; Vijayagopal, R.; Stutenberg, K.; Rousseau, A. Vehicle level control analysis for Voltec powertrain. *World Electr. Veh. J.* **2018**, *9*, 29. [CrossRef]
30. Zhuang, W.; Zhang, X.; Li, D.; Wang, L.; Yin, G. Mode shift map design and integrated energy management control of a multi-mode hybrid electric vehicle. *Appl. Energy* **2017**, *204*, 476–488. [CrossRef]
31. Park, J.Y.; Park, Y.K.; Park, J.H. Optimal power distribution strategy for series-parallel hybrid electric vehicles. *Proc. Inst. Mech. Eng. Part D J. Automob. Eng.* **2008**, *222*, 989–1000. [CrossRef]
32. Ahn, K.; Cho, S.; Cha, S.W.; Lee, J.M. Engine operation for the planetary gear hybrid powertrain. *Proc. Inst. Mech. Eng. Part D J. Automob. Eng.* **2006**, *220*, 1727–1735. [CrossRef]
33. Cammalleri, M.; Rotella, D. Functional design of power-split CVTs: An uncoupled hierarchical optimized model. *Mech. Mach. Theory* **2017**, *116*, 294–309. [CrossRef]
34. Rotella, D.; Cammalleri, M. Direct analysis of power-split CVTs: A unified method. *Mech. Mach. Theory* **2018**, *121*, 116–127. [CrossRef]
35. Rotella, D.; Cammalleri, M. Power losses in power-split CVTs: A fast black-box approximate method. *Mech. Mach. Theory* **2018**, *128*, 528–543. [CrossRef]
36. Cammalleri, M.; Castellano, A. Analysis of hybrid vehicle transmissions with any number of modes and planetary gearing: Kinematics, power flows, mechanical power losses. *Mech. Mach. Theory* **2021**, *162*, 104350. [CrossRef]
37. Conlon, B.M.; Blohm, T.; Harpster, M.; Holmes, A.; Palardy, M.; Tarnowsky, S.; Zhou, L. The Next Generation "voltec" Extended Range EV Propulsion System. *SAE Int. J. Altern. Powertrains* **2015**, *4*, 248–259. [CrossRef]
38. Jurkovic, S.; Rahman, K.; Patel, N.; Savagian, P. Next Generation Voltec Electric Machines; Design and Optimization for Performance and Rare-Earth Mitigation. *SAE Int. J. Altern. Powertrains* **2015**, *4*, 336–342. [CrossRef]
39. Anwar, M.; Hayes, M.; Tata, A.; Teimorzadeh, M.; Achatz, T. Power dense and robust traction power inverter for the second-generation chevrolet volt extended-range EV. *SAE Int. J. Altern. Powertrains* **2015**, *4*, 145–152. [CrossRef]